BEEF-vdW+U method applied to perovskites: Thermodynamic, structural, electronic, and magnetic properties

Yang Li[1], Ya-Shan Zheng[1], Yi-An Zhu[1,*], Zhi-Jun Sui[1], Xing-Gui Zhou[1], De Chen[2], and Wei-Kang Yuan[1]

[1] UNILAB, State Key Laboratory of Chemical Engineering, East China University of Science and Technology, Shanghai 200237, China
[2] Department of Chemical Engineering, Norwegian University of Science and Technology, N-7491 Trondheim, Norway

* E-mail: yanzhu@ecust.edu.cn

Abstract

The recently developed BEEF-vdW exchange-correlation method provides a reasonably reliable description of both long-range van der Waals interactions and short-range covalent bonding between molecules and surfaces. However, this method still suffers from the excessive electron delocalization that is connected with the self-interaction error and, consequently, the calculated chemical and physical properties such as formation energy and band gap deviate markedly from the experimental values, especially when strongly correlated systems are under investigation. In this contribution, BEEF-vdW+U calculations have been performed to study the thermodynamic, structural, electronic, and magnetic properties of La-based perovskites. An effective interaction parameter U_{eff} and an energy adjustment ΔE_M are determined simultaneously by a mixing GGA and GGA+U method, where the enthalpy or Gibbs free energy of formation of oxides containing a transition metal in different oxidation states are fitted to available experimental data. The ΔE_M is found to have its origin in the fact that the GGA+U method gives rise to the offsets in the total energy that include not only the desired physical correction but also an arbitrary contribution. Calculated results indicate that the BEEF-vdW method provides a more accurate description of the bonding in the O_2 molecule than the PBE method and has generally smaller U_{eff} values for the 3*d*-block transition metals, thereby giving rise to band gaps and magnetic moments that are in better agreement with the experimentally measured values.

Keywords: GGA+U; Perovskite; Formation energy; Band gap; Magnetic moment

Supplementary data for this article is available

1. INTRODUCTION

Density functional theory (DFT) has gained considerable ground in recent years, and has become one of the most powerful techniques for predicting the structure and property of molecules and extended solids. [1] In contrast to the Hartree-Fock approach which does not include electron correlation, DFT has its complexity and a lot of physics hidden inside the approximate exchange-correlation functional. This term works surprisingly well given its simplicity and holds the key to the success of the theory. On the other hand, the commonly used LDA/GGA suffers from the delocalization error arising from the Coulomb term that pushes electrons apart (previously known as the "self-interaction error") and the static correlation error which is due to the failure of the description of degenerate and near-degenerate states [2]. The former is believed to be connected

with the spurious interaction of an electron with itself, which can be cancelled by an equivalent term in the exchange energy in the Hartree-Fock approach. In the DFT method, however, the exact exchange-correlation functional is still unknown and, consequently, its accuracy in determining chemical and physical properties of materials depends strongly on the degree of the cancellation of errors in energy differences.

The "self-interaction error" in the occupied states may lead to excessive electron delocalization and, consequently, to an increase in the occupied electronic energy levels [3]. This deficiency in LDA/GGA is largely responsible for the underestimation of band gap by DFT calculations, especially in strongly correlated systems that possess highly localized *d* or *f* electrons. When electrons are transferred between species in different chemical environments, just as in the case of oxidation of transition metal cations, the "self-interaction error" would penalize the low oxidation state over the higher one, as the latter has less localized *d* orbitals occupied. For this reason, little error cancellation is expected and the resultant oxidation energies are invariably overestimated [4].

To give a reasonably accurate description of the electronic structures as well as energetics of transition metal oxides, several new approaches, including LDA/GGA+U [5, 6], hybrid functional [7], and random phase approximation (RPA) [8], have been developed to address the transition between localized and delocalized electronic states. Among them the LDA/GGA+U framework offers the best compromise between accuracy and computational efficiency. In this method, the essential assumption is that the strongly correlated *d* or *f* electrons are subject to on-site quasi-atomic interactions which can be described by a Hubbard term U and a Hund's-rule exchange term J [5, 6]. A simplified (rotationally invariant) approach to LDA/GGA+U was proposed by Dudarev et al. [9], in which an effective interaction parameter $U_{eff} = U - J$, was introduced by adding a penalty function to the total energy expression in LDA/GGA. This additional Hubbard-type term localizes the electronic states to which it is applied and thus lowers the energy of the occupied states.

It is well known that the accuracy of the LDA/GGA+U method depends entirely on the U_{eff} for transition metal elements. Determining an appropriate U_{eff}, however, can be quite tricky. Although some researchers have pointed out that purely theoretical calculations can be used in this regard [10], the method proves to be difficult to apply to all transition metal oxides, such as CeO_2 [11]. In practice, the U_{eff} values are often obtained by fitting calculated band gap and thermodynamic quantities to available experimental data [12-14]. One problem with such a determination is the difficulty of ensuring that the fitting to one property can correctly reproduce others. Moreover, it was recently found that the U_{eff} value depends upon not only the identity of transition metal elements but also upon their local environments, such as the oxidation state and surrounding ligands [15]; that is, the transferability of U_{eff} across compounds containing transition metal ions is limited. Finally, the U_{eff} values obtained by different calculation methods (e.g., by using different exchange-correlation functionals and pseudopotentials) are not always the same. Thus, when the calculation method is changed, it is highly required to repeat the fitting to a specific property of interest to give a reasonable U_{eff} value for a particular system.

Recently, Wellendorff et al. developed a semilocal approximation with an additional nonlocal correlation term, the Bayesian error estimation functional with van der Waals correlation (BEEF-vdW) [16], using regularization and crossover point-validation methods from machine learning. By taking a linear combination of local (Perdew-Wang LDA) [17], semilocal (PBE) [18], and nonlocal correlation (vdW-DF2) [19] as the correlation model space, both a reasonably reliable description of long-range van der Waals forces and a quantitatively accurate prediction of short-range covalent bonding between molecules and surfaces can be achieved, making BEEF-vdW an excellent density functional for studies in heterogeneous catalysis and surface science. However, the self-interactions of electrons with themselves that arise from the Hartree term are still not fully compensated for in the BEEF-vdW method and, consequently, an appropriate correction to the functional (e.g., GGA+U) also needs to be made when strongly correlated systems are under investigation.

Perovskite-type oxides, which have a general formula ABO_3, represent an ideal system for ascertaining the relationship between chemical composition and electronic structure of materials, as their extraordinary ability allows doping and substitution for both the *A*- and the *B*-site cations while retaining the structural integrity [20]. Meanwhile, the chemical diversity makes it possible to tailor various properties of perovskites to a wide variety of applications, including cathode materials in solid oxide fuel cells (SOFCs) [21], catalysts in heterogeneous catalysis [22], oxygen sources in membrane separation [23], and high-temperature oxygen sensors [24]. Since the *B*-site cations usually come from *d*-block transition metals, it is well established that most perovskite-centered transition-metal oxides have localized *d* electrons. Although research efforts have previously been devoted to probing the geometrical and electronic structures of perovskites using the GGA+U method [25-30], none of them have been focused on the determination of the U_{eff} values for DFT investigation of vdW-type, which makes it challenging to simultaneously account for strong and weak interactions present in condensed matter physics and surface chemistry. In this contribution, BEEF-vdW+U calculations have been carried out to obtain the thermodynamic, structural, electronic, and magnetic properties of $LaMO_3$ (M = *Sc* - *Cu*). The O_2 binding error is first corrected by fitting the energetics of formation of nontransition-metal oxides to the experimental values. Then, an effective interaction parameter U_{eff} and an energy adjustment ΔE_M are determined simultaneously by a mixing GGA and GGA+U method. Finally, we calculate other physical properties of $LaMO_3$ by using the derived U_{eff} values

and conclude by discussing the agreement between the calculated and experimental results.

2. METHODOLOGY

2.1 DFT calculations and thermodynamic corrections

All periodic DFT calculations have been carried out with the VASP software package [31], in which the wavefunction at each k-point is expanded in terms of a plane wave basis set. The projector-augmented wave (PAW) method was employed to represent the interactions between ion cores and valence electrons [32] and both the BEEF-vdW [16] and the PBE methods [18] were used to account for the exchange and correlation of the Kohn-Sham theory. The application of the PBE method was to validate the data obtained using the BEEF-vdW method and hence to evaluate the reliability of the computational methods, as PBE is by far the most widely used GGA method. By using the "hard" PAW potentials with valence configurations *La* ($5s^2\ 5p^6\ 6s^2\ 5d^1$), *O_s* ($2s^2\ 2p^4$), *Sc_sv* ($3s^2\ 3p^6\ 4s^2\ 3d^1$), *Ti_pv* ($3p^6\ 3d^2\ 4s^2$), *V_sv* ($3s^2\ 3p^6\ 3d^3\ 4s^2$), *Cr_pv* ($3p^6\ 3d^5\ 4s^1$), *Mn_pv* ($3p^6\ 3d^5\ 4s^2$), *Fe_pv* ($3p^6\ 3d^6\ 4s^2$), *Co* ($3d^7\ 4s^2$), *Ni_pv* ($3p^6\ 3d^8\ 4s^2$), and *Cu* ($3d^9\ 4s^2$), a plane-wave energy cutoff of up to 600 eV was necessary to converge the total energy per atom in $LaMO_3$ to within 1 meV. Sampling of the Brillouin zone was performed with the Monkhorst-Pack method [33] and electronic occupancies were determined according to the Gaussian scheme with an energy smearing of 0.1 eV. A gamma-centered 11 × 11 × 11 *k*-point grid was used to sample the Brillouin zone of the $LaMO_3$ perovskites adopting an orthorhombic structure, and sampling of the Brillouin zone of the rhombohedral structure was performed with a 7 × 7 × 5 grid. For the majority of this work, spin-polarized calculations were performed to obtain reasonably accurate structures and energetics of the transition metal-based perovskites. During geometry optimization of the bulk structures of transition metal oxides, a quasi-Newton algorithm was used, and both the atomic coordinates and lattice vectors are allowed to fully relax until the forces on each atom are converged better than 0.01 eV/Å.

The mass-weighted Hessian matrix was calculated under the finite difference approximation and diagonalized to give the vibrational frequencies of the normal nodes. Then, the enthalpy and Gibbs free energy of molecular O_2 at a temperature T and a pressure P were calculated in the ideal-gas limit:

$$H_{O_2}(T,P) = E_{O_2} + E_{ZPE} + \Delta H^\circ(0 \to T) \tag{1}$$

$$\begin{aligned} G_{O_2}(T,P) &= H_{O_2} - T \cdot S(T,P) \\ &= H_{O_2} - T \cdot S^\circ(T,P) + RT \ln\left(\frac{P}{P^\circ}\right) \end{aligned} \tag{2}$$

where E_{O_2} is the total energy of molecular O_2 as determined by DFT calculations. E_{ZPE} is the zero-point energy, and $\Delta H^\circ(0 \to T)$ is the enthalpy change from 0 K to temperature T. As for the transition-metal oxide crystal structures, all degrees of freedom were treated in the harmonic limit and the Gibbs free energy can therefore be written as

$$G_{oxide}(T,P) = E_{oxide} + E_{ZPE} + \Delta U^\circ(0 \to T) - T \cdot S^\circ(T) \tag{3}$$

where $\Delta U^\circ(0 \to T)$ is the change in internal energy from 0 K to temperature T. A more detailed derivation of the thermodynamic properties can be found in our previous work [34].

2.2 GGA+U framework

Here the enthalpy and Gibbs free energy of formation of transition metal oxides were calculated and compared with available experimental data to determine the U_{eff} values, which were subsequently used to reproduce physical properties of *La*-based perovskites. As pointed out by Wang et al. [4], the error in the oxidation energy of transition-metal oxides has contributions from both the overestimation of the binding energy in the O_2 molecule by LDA/GGA and the failure in the cancellation of the "self-interaction error" in the energy difference. The O_2 binding energy can be corrected by fitting the energetics of formation of nontransition-metal oxides to experimental values, [4] and the correlation error may be removed by using a Hubbard-type term to address the on-site Coulomb interaction in the localized orbitals. It should be noted that this method is only applicable to the situation where the *d* orbital is atomic-like, e.g., in the oxidation of a low-valent oxide to a higher one [4]. If the formation enthalpy of transition-metal oxides is concerned, however, an additional correction needs to be made to account for the energy change accompanying the transition from the delocalized electronic states to the localized states. A methodology mixing GGA and GGA+U calculations have been proposed by Jain et al. [35], in which the overall reaction for the formation of $FeAl_2O_4$ was decomposed into three reactions and the total energies of the element/compound with uncorrelated and correlated *d* states were computed with GGA and GGA+U, respectively. By fitting the calculated formation energy of Fe_2O_3 to the experimental value, an energy adjustment that is proportional to the transition metal content in the compound was obtained. Of the three errors, the O_2 binding error and the absence of the aforementioned energy adjustment underestimate the formation enthalpy of transition-metal oxides (less negative) while the correlation error overestimates the formation enthalpy (more negative). As a consequence, the accuracy of the predication about the formation enthalpy depends strongly upon how the three contributions counteract one another.

Armed with this knowledge, we can calculate the enthalpy change ($\Delta H^{Exp}_{f,M_xO_y}$) for a transition-metal oxide formation reaction

$$xM + \frac{y}{2}O_2 \to M_xO_y \tag{4}$$

as

$$\Delta H_{f,M_xO_y}^{Exp} = H_{M_xO_y}^{GGA+U} - x\cdot\Delta E_M - x\cdot H_{M_{delocalized}}^{GGA} - \frac{y}{2}\cdot\left(H_{O_2}^{GGA} + \Delta E_{O_2}\right) \quad (5)$$

where $H_{M_xO_y}^{GGA+U}$, $H_{M_{delocalized}}^{GGA}$, and $H_{O_2}^{GGA}$ are the enthalpies of M_xO_y, M metal, and molecular O_2 as calculated by GGA+U and GGA, respectively, ΔE_{O_2} is the energy correction to the O_2 binding energy, and ΔE_M is the energy adjustment that needs to be made to the total energies by GGA+U so that the energetics obtained from the mixing GGA and GGA+U calculations are comparable. Because the ΔE_M has its origin in the fact that the GGA+U method gives rise to the offsets in the total energy that include not only the desired physical correction but also an arbitrary contribution [36], it can be expressed as

$$\Delta E_M = \frac{1}{x}\cdot\left[\Delta H_{f,M_xO_y}^{GGA} + \Delta E\left(U_{eff}\right) - \Delta H_{f,M_xO_y}^{Exp}\right] \quad (6)$$

where $\Delta H_{f,M_xO_y}^{GGA}$ represents the formation enthalpy of the transition-metal oxide M_xO_y determined purely by GGA, which is given by the expression

$$\Delta H_{f,M_xO_y}^{GGA} = H_{M_xO_y}^{GGA} - x\cdot H_{M_{delocalized}}^{GGA} - \frac{y}{2}\cdot\left(H_{O_2}^{GGA} + \Delta E_{O_2}\right) \quad (7)$$

and $\Delta E\left(U_{eff}\right)$ represents the energy correction to the correlation error, which is defined as

$$\Delta E\left(U_{eff}\right) = H_{M_xO_y}^{GGA+U} - H_{M_xO_y}^{GGA} \quad (8)$$

In light of this information, Eq. (5) can be rewritten as

$$\Delta H_{f,M_xO_y}^{Exp} = \left[H_{M_xO_y}^{GGA+U} - x\cdot H_{M_{localized}}^{GGA+U} - \frac{y}{2}\cdot\left(H_{O_2}^{GGA} + \Delta E_{O_2}\right)\right] + x\cdot\left[\left(H_{M_{localized}}^{GGA+U} - \Delta E_M\right) - H_{M_{delocalized}}^{GGA}\right] \quad (9)$$

where the first term on the right-hand side of the equation represents the enthalpy change for the oxidation of the transition metal in a "virtual" reduced state that has localized *d* electrons to an oxide where the transition metal has a positive oxidation number. Since the *d* electrons are strongly correlated in both the reactant and the product, the reaction enthalpy is calculated purely by the GGA+U method. The second term on the right-hand side of the equation can be envisioned as the energy required for the transition of the *d* electrons in the reduced metal from the delocalized state to the localized state. Upon the decomposition and rearrangement of the equation, it is clear that the ΔE_M depends solely on the electronic structure of the transition metal and does not vary with the identity of the transition-metal oxides under investigation. For the transition-metal oxides that have no tabulated values for the formation enthalpy, the Gibbs free energy of formation ($\Delta G_{f,M_xO_y}$) is calculated instead:

$$\Delta G_{f,M_xO_y} = G_{M_xO_y}^{GGA+U} - x\cdot\Delta E_M - x\cdot G_{M_{delocalized}}^{GGA} - \frac{y}{2}\cdot\left(G_{O_2}^{GGA} + \Delta E_{O_2}\right) \quad (10)$$

As stated in the Introduction, for a given transition metal element, the fitted U_{eff} value may vary with the oxidation state and the property of interest. From Eqs. (5) and (10), it follows that this dependence holds true for the ΔE_M, which changes with the U_{eff} value so as to keep the calculated thermodynamic properties close to the experimental results.

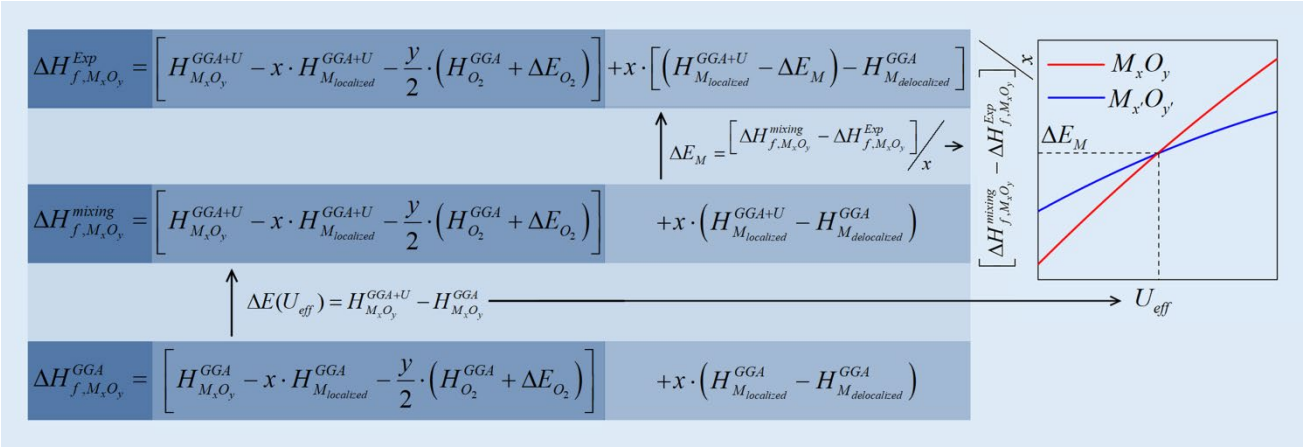

Figure 1. Illustration of the methodology for the fitting of U_{eff} and ΔE_M. The $\Delta H_{f,M_xO_y}^{mixing}$ and $\Delta H_{f,M_xO_y}^{GGA}$ are the formation enthalpy of the transition-metal oxide M_xO_y calculated purely by the mixing method and by GGA, respectively. The $\Delta E(U_{eff})$ is the energy correction to the correlation error, which is defined as the difference in the calculated enthalpy of the oxide M_xO_y by GGA+U and by GGA. The ΔE_M is the energy adjustment that needs to be made to the total energies by GGA+U so that the energetics obtained from the mixing calculations are comparable.

Table 1. Crystal and magnetic structures as well as thermodynamic properties of La-based perovskites and binary metal oxides.

Oxide	Space group	ICSD	Magnetic structure	Enthalpy of formation at 298 K (eV) [37]	Gibbs free energy of formation at 298 K (eV) [37]
$LaScO_3$	*Pbnm*	99538	NM [38]	-19.56 [39]	-
$LaTiO_3$	*Pbnm*	98414	GAFM [40]	-17.62 [41]**	-
$LaVO_3$	*Pbnm*	73899	CAFM [40]	-16.20 [42]	-15.37 [42]
$LaCrO_3$	*Pbnm*	153615	GAFM [40]	-15.92 [43]	-
$LaMnO_3$	*Pbnm*	56616	AAFM [40]	-14.90 [42]	-
$LaFeO_3$	*Pbnm*	78062	GAFM [40]	-14.31 [43]	-
$LaCoO_3$	$R\bar{3}c$	201762	FM	-12.87 [43]	-
$LaNiO_3$	$R\bar{3}c$	93919	FM	-12.36 [43]	-
$LaCuO_3$	$R\bar{3}c$	73554	NM	-	-10.62 [44]**
Sc_2O_3	$I\bar{4}a$	-	NM	-19.78	-18.85*
TiO_2	$P4_2/mnm$	51939	NM	-9.79	-9.22
VO	$Fm\bar{3}m$	647611	AFM [45]	-4.48	-4.19
V_2O_3	$R\bar{3}c$	33641	AFM [46]	-12.63	-11.80
VO_2	$P2_1/C$	15889	FM	-7.40	-6.83
Cr_2O_3	$R\bar{3}c$	75577	AFM [47]	-11.76	-10.91
CrO_2	$P4_2/mnm$	35327	FM [48]	-6.20	
MnO	$Fm\bar{3}m$	53928	AFM [49]	-3.96	-3.76*
Mn_2O_3	*Pbca*	9090	AFM [50]**	-9.94	
FeO	$Fm\bar{3}m$	53519	FM [49]	-2.82	-2.61
Fe_2O_3	$R\bar{3}c$	71994	AFM [47]	-8.56	-7.71
CoO	$Fm\bar{3}m$	9865	AFM [49, 51]	-2.46	-2.22
NiO	$Fm\bar{3}m$	76669	AFM [49]	-2.48	-2.21
CuO	*C*2/*C*	628618	AFM [52]	-1.62	-1.33
Li_2O	$P4_2/mnm$	51939	NM	-6.21	-5.83
Na_2O	$Fm\bar{3}m$	87177	NM	-4.33	-3.92
MgO	$R\bar{3}c$	77696	NM	-6.23	-5.90
Al_2O_3	*P*3*m*1	154586	NM	-17.37	-17.68
SiO_2	$P4_2/mnm$	15889	NM	-9.44	-8.88
CaO	*P*3*m*1	160203	NM	-6.58	-6.25

*Experimental Gibbs free energy of formation at 300 K obtained from Smithells metals reference book [53].

**Estimated enthalpy or Gibbs free energy of formation by using an empirical method.

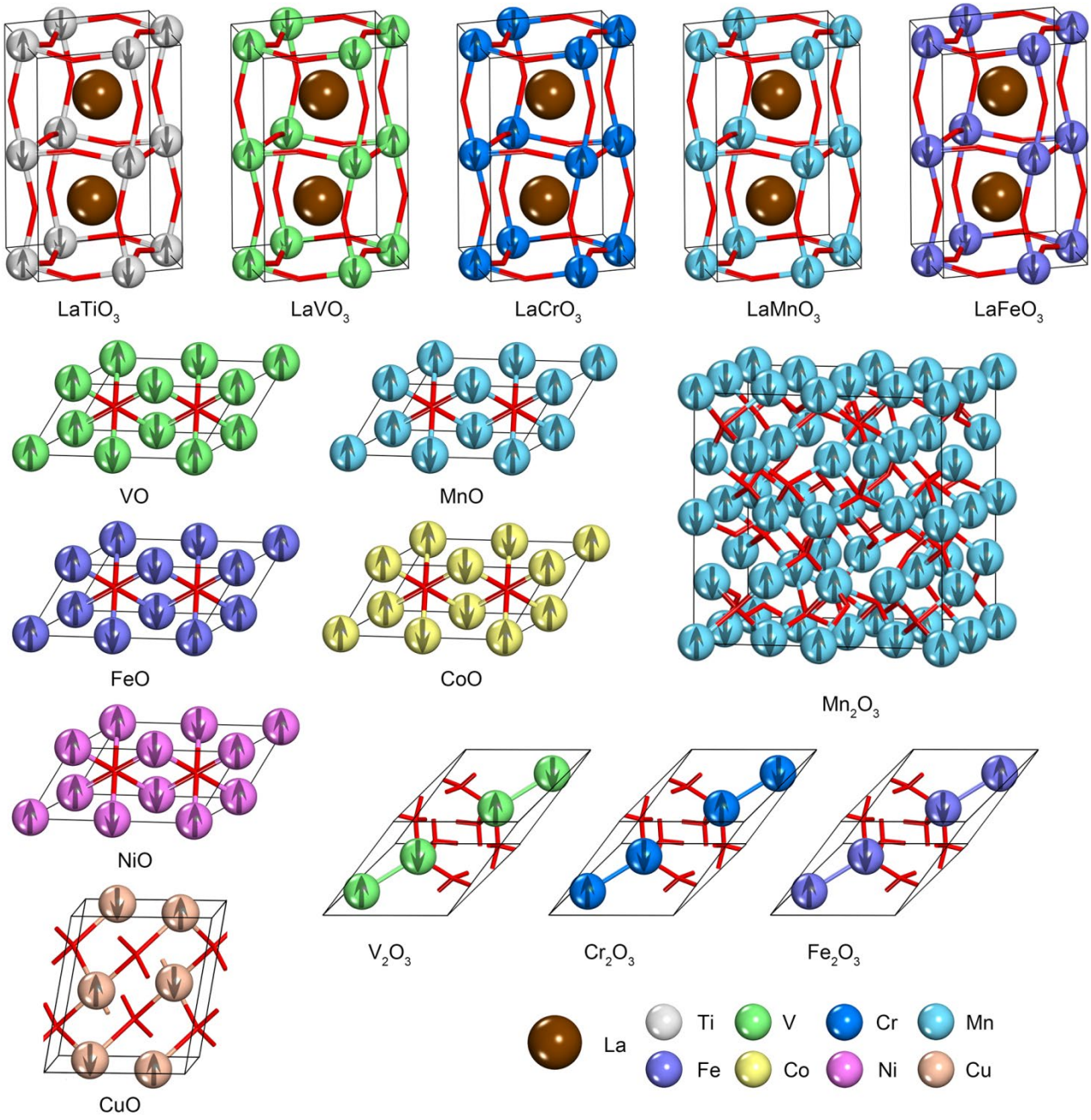

Figure 2. Schematic representations of magnetic structures of antiferromagnetic substances.

However, despite having different possible values, the fitted U_{eff} for the oxides of each transition-metal element was found to lie within a narrow range and the averaged U_{eff} can often improve dramatically the description of other physical properties such as band gap and magnetic moment [4]. Hence, it is technically feasible to simultaneously determine a single value of U_{eff} and ΔE_M for each transition-metal element by fitting the enthalpy or Gibbs free energy of formation of oxides containing that metal in different oxidation states. In practice, we plotted the energy difference (on a *per* mol metal basis) between the experimentally and theoretically determined thermodynamic properties as a function of the U_{eff}, and the intersection of the curves defines the U_{eff} and ΔE_M that are transferable between the oxides. From this point of view, our method is quite different from the methodology used by Jain et al. [35], where the oxidation energy of a low-valent oxide to a higher one was first fitted to derive the U_{eff} value and the ΔE_M was then obtained by mixing GGA and GGA+U calculations. When more than one intersection point is obtained, the U_{eff} takes the value that may give rise to a closer band gap of the transition-metal oxides to the experimental data. The detailed methodology is illustrated in figure 1.

2.3 Selection of materials

In addition to the *La*-based perovskites $LaMO_3$ (*M* = *Sc* - *Cu*), a number of binary metal oxides that contain transition metals with a +2, +3, and +4 oxidation number were chosen to determine the U_{eff} value for each transition-metal element. $LaZnO_3$ was not included in the present work because 3*d* orbitals become more significantly contracted across the transition metal series, making it impossible to remove electrons from the 3*d* orbitals of *Zn* to form stable Zn^{3+} cations [54]. At room temperature the *La*-based perovskites may adopt either an orthorhombic or a rhombohedral structure with the *Pbnm* (*M* = *Sc* - *Fe*) or $R\bar{3}c$ (*M* = *Co* - *Cu*) space group symmetry [55]. As for the binary oxides, most monoxides and dioxides adopt a cubic and a tetragonal structure, respectively, while the oxides containing metals in the +3 oxidation state tend to crystalize with a structure that has a primitive rhombohedral lattice (see table 1). The crystal symmetries, however, can be lowered or removed by specifying initial spin polarization on the transition-metal cations. Here the experimentally observed magnetic structures were adopted for most of the transition-metal oxides applied, as summarized in table 1. In particular, the magnetic configurations of the antiferromagnetic substances are shown schematically in figure 2.

The thermodynamic properties of the metal oxides at specified temperatures are also presented in table 1. Of the $LaMO_3$ perovskites, $LaTiO_3$ and $LaCuO_3$ have no experimental value available for the enthalpy and Gibbs free energy of formation. Thus, the values were estimated by using empirical methods. As for $LaTiO_3$, Cheng et al. [39] proposed that the reaction enthalpy for $\frac{1}{2}La_2O_3+\frac{1}{2}M_2O_3 \rightarrow LaMO_3$ can be approximated by an empirical expression:

$$\Delta H_r = 630 - 720 \cdot t_p \tag{11}$$

where t_p is the Goldschmidt tolerance factor of the perovskite, which is defined as

$$t_p = \frac{r_A + r_O}{\sqrt{2}\left(r_B + r_O\right)} \tag{12}$$

where r_A, r_B, and r_O are the ionic radii of A-, B-site cation, and oxygen anion, respectively. Since the experimental formation enthalpies of La_2O_3 and Ti_2O_3 are already known, the formation enthalpy of $LaTiO_3$ can be readily obtained [41]. For $LaCuO_3$, however, this method is not applicable because Cu_2O_3 has not yet been isolated as a pure substance. Given the fact that the structural stabilities (and hence the formation energies) of the metal oxides decrease with decreasing the actual partial charges on the cations and anions [56], Sreedharan et al. [44] estimated the Gibbs free energy of formation of $LaCuO_3$ at a given temperature by first plotting the Gibbs free energy of formation of $LaMO_3$ (*M* = *Mn*, *Fe*, *Co*, and *Ni*) against the atomic number of the transition metal and then extrapolating linearly to $LaCuO_3$. In this way, an empirical relationship that relates the thermodynamic property of $LaCuO_3$ to temperature was developed:

$$\Delta G_{f,LaCuO_3} = -1095.0 + 0.2350 \cdot T \tag{13}$$

3. RESULTS AND DISCUSSION

3.1 Correction to oxygen binding energy

As aforementioned, there exist three contributions to the error in the calculated formation energies of transition-metal oxides by LDA/GGA. Unlike the other two contributions, the overbinding in the O_2 molecule represents a constant shift in the calculated values, making the formation energies of oxides less negative than are obtained experimentally. The overbinding cannot be cancelled because the metal-oxygen bond that results is strongly polar, with little covalent character, and it is often sufficient to assume that the interaction between them is entirely electrostatic in character. By fitting the calculated energetics of formation of nontransition-metal oxides to the experimental values, it is found that the correction to the O_2 binding energy depends strongly on the calculation method used and the thermodynamic property of interest. For instance, if the experimental formation enthalpy is plotted against the value calculated by the BEEF-vdW and PBE methods, it is clear that the total energy of molecular O_2 is overestimated by 0.46 and 0.84 eV respectively, as shown in figure 3a. However, in the cases where the Gibbs free energy of formation is concerned, the energy corrections are predicted to be 0.37 eV for BEEF-vdW and 0.74 eV for PBE. It can be seen that the BEEF-vdW method gives a more accurate description of the bonding in the O_2 molecule, which is probably due to the fact that the BEEF-vdW method has been optimized by using several training data sets that include the formation energy of molecular O_2 and the energy changes for molecular reactions involving O_2 as a reactant.

On the other hand, even after the total energy of O_2 has been corrected to account for the O_2 binding error, there remains a discrepancy between the calculated and experimental O_2 binding energy, as can be seen in table 2. Previously, Wang et al. [4] used the same method to make the least squares fit, and the formation energies of nontransition-metal oxides were calculated by using the PBE method and the standard version of the PAW potential for *O*. An energy

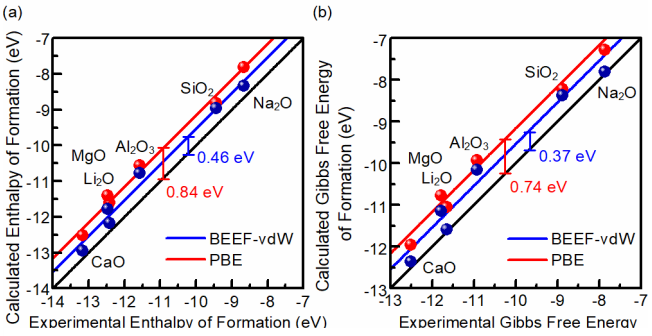

Figure 3. Calculated (a) enthalpy and (b) Gibbs free energy of formation of nontransition-metal oxides (*per* mol O_2 at 298 K) as a function of the experimental value.

Table 2. Experimental and calculated oxygen binding energies by the BEEF-vdW and PBE methods.

Experimental O_2 binding energy (eV)	Calculated O_2 binding energy by BEEF-vdW (eV)			Calculated O_2 binding energy by PBE (eV)		
	Uncorrected	Corrected Fitting H	Fitting G	Uncorrected	Corrected Fitting H	Fitting G
-5.23 [18]* -5.12 [57]	-5.68	-5.22	-5.31	-6.19	-5.35	-5.45

*Experimental O_2 binding energy with zero-point energy removed.

correction of 1.36 eV was obtained in their work, and the oxygen binding energy was corrected to -4.66 eV, which becomes less negative than the experimental value. They believed that this additional deviation is related to the electron transfer from the metal *s* and/or *p* states to the oxygen 2*p* orbital when O_2 is reduced to form O^{2-}.

3.2 Determination of U_{eff} and ΔE_M

3.2.1 Lanthanum

La-based perovskites $LaMO_3$ (M = *Sc* - *Cu*) constitute one of the best known classes of ternary transition-metal oxides. Apart from the period 3 elements, another transition metal, La, is also involved in the compounds. It was reported that although the *La* 4*f* electrons show strong intra-atomic Coulomb correlations in the $LaMO_3$ perovskites [58], the *La* 5*d* electrons are only weakly correlated because there are a large number of electron holes in the 5*d* orbitals of La^{3+}, which gives rise to a strong hybridization between the *La* 5*d* electrons and the *O* 2*p* electrons [59]. Since the 4*f* states are not involved in the valence configurations of the PAW potential for *La* and the 5*d* states in La^{3+} are weakly localized, the electronic structures of *La*-based metal oxides are calculated without applying any U_{eff} value to the electronic states in the *La* cation. To demonstrate that this treatment is reasonably accurate, it is useful to make a first test by calculating the enthalpy change for the reaction,

$$La + \frac{1}{2}M_2O_3 + \frac{3}{4}O_2 \rightarrow LaMO_3 \qquad (14)$$

where *La* reacts with M_2O_3 (M = *Sc*, *V*, *Cr*, *Mn*, and *Fe*) and molecular oxygen to form the $LaMO_3$ perovskites. In this reaction, the SIE associated with the localized *d* states in the *M* cations is believed to be cancelled out because the *M* cations in M_2O_3 and $LaMO_3$ have nearly the same chemical environment and oxidation number. The deviations of the calculated reaction enthalpies from the experimental data (with the error in the oxygen binding energy removed) are averaged to 0.08 eV for BEEF-vdW and 0.10 eV for PBE on a *per* mol metal basis, which are reasonably small and within the uncertainty of DFT calculations.

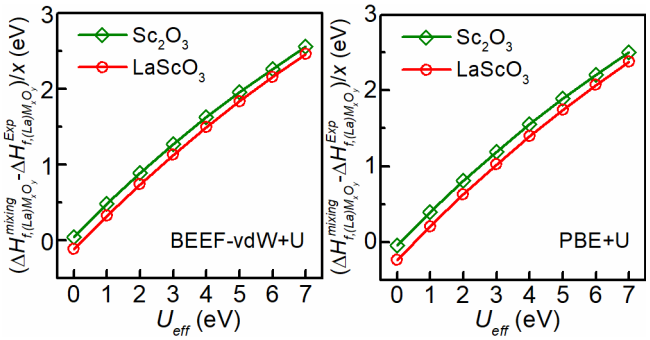

Figure 4. Differences between the calculated and experimental enthalpies of formation of *Sc*-based oxides as a function of U_{eff}.

3.2.2 Scandium oxide

As noted earlier, the U_{eff} and ΔE_M values for each transition metal in period 3 can be obtained by first plotting $\left(\Delta H^{mixing}_{f,(La)M_xO_y} - \Delta H^{Exp}_{f,(La)M_xO_y}\right)/x$ or $\left(\Delta G^{mixing}_{f,(La)M_xO_y} - \Delta G^{Exp}_{f,(La)M_xO_y}\right)/x$ against the U_{eff} value for the oxides containing the metal in different oxidation states and then identifying the intersection points of the curves. However, since *Sc* occurs only in the +3 oxidation state, where the 3+ ion with an [*Ar*] configuration is particularly stable, it is technically unfeasible to obtain the U_{eff} value by calculating the enthalpy change for oxidation reactions. Indeed, if we plot the energy difference as a function of the U_{eff} value for Sc_2O_3 and $LaScO_3$, two parallel curves are observed, without any intersection point (see Figure 4).

On the other hand, it was reported that the degree of localization of 3*d* electrons in the transition-metal oxides can be traced to the competition between Coulomb repulsion which makes 3*d* electrons more localized and the hybridization of metal 3*d* states with *O* 2*p* states that delocalizes 3*d* orbitals [60]. Because *Sc* is positioned at the beginning of the first transition series, it is often sufficient to assume that the metal-ligand interaction in its compounds is entirely electrostatic in character. As a result, although the calculated formation enthalpy of $LaScO_3$ by BEEF-vdW and PBE is 0.12 and 0.23 eV, respectively, more negative than the experimental data, introduction of a penalty function to address excessive electron delocalization that arises from the SIE seems not necessary.

3.2.3 Titanium oxide

The thermodynamic property of TiO_2 and $LaTiO_3$ is used to determine the U_{eff} value for *Ti* because Ti_2O_3 has strongly fluctuating orbitals [61] that cannot be accurately described by GGA+U [62]. Although $LaTiO_3$ has only a band gap of 0.1 - 0.2 eV [59, 63], it is an anti-ferromagnetic Mott-Hubbard insulator due to strong on-site Coulomb repulsion [64], and the weakly fluctuating orbitals make GGA+U an appropriate approach for this material. As expected, the resulting U_{eff} for *Ti* is rather small (0.6 eV for BEEF-vdW+U and 1.3 eV for PBE+U in figure 5a), indicating that the effective hybridization strength is comparable to the Coulomb interaction between 3*d* electrons [40]. It should be noted that Aykol et al. [15] obtained a U_{eff} value of 4.35 eV on the basis of the thermodynamic quantities of Ti_2O_3 and TiO_2. However, applying such a high U_{eff} value gives a band gap that is ~1.5 eV higher than the experimental value for Ti_2O_3. Closer examination of their calculated dependence of the energy difference on the U_{eff} indicates that the abnormally high slope of the curve referring to Ti_2O_3 could be responsible for the deviation.

3.2.4 Vanadium oxide

Figure 5b shows the energy difference of *VO*, V_2O_3, VO_2, and $LaVO_3$ as a function of U_{eff}, where the U_{eff} ranges from 0 eV to 7 eV. Given the diversity in the oxidation state of *V* in its oxides, it is not surprising to learn that there exist several distinctly different intersection points of the curves. Furthermore, the calculated U_{eff} spans a wide range of values, varying from 2.5 eV to 4.3 eV for BEEF-vdW and from 3.0 eV to 5.8 eV for PBE, in accord with the PBE results obtained by Aykol et al. [15] and by Lutfalla et al. [65]. Thus, one problem with the determination of the U_{eff} value for *V* is the difficulty of obtaining the correct band structures of different metal oxides by applying a single U_{eff}. For this reason, unlike for the other 3*d*-block transition metals, the U_{eff} value for *V* in $LaVO_3$ is determined by further comparing the calculated band gaps given by all the possible U_{eff} values to available experimental data. It is eventually found that the intersection point of the curves referring to VO_2 and $LaVO_3$ defines the appropriate U_{eff} values (2.5 eV for BEEF-vdW+U and 3.0 eV for PBE+U) that provide a reasonably accurate estimate of the band gap of $LaVO_3$.

3.2.5 Chromium, manganese, iron, cobalt, nickel, and copper oxides

The data for the *Cr*-, *Mn*-, *Fe*-, *Co*-, *Ni*-, and *Cu*-based oxides are shown in figure 5c-h. It can be seen from the figure 5c-h that the energy difference at U_{eff} = 0 becomes more positive as the transition metal has a lower oxidation number, because the SIE penalizes the low oxidation state over the higher one. Furthermore, the curves for the metal oxides containing the metal in the same formal oxidation state are almost coincident with each other, which can be explained by their similar octahedral coordination environments. For instance, the dependence of the energy differences for Cr_2O_3 and $LaCrO_3$ on the U_{eff} value follows nearly the same trend. As another example, the curve for Fe_2O_3 closely resembles that for $LaFeO_3$, regardless of the exchange-correlation functional used. The only exception occurs for Mn_2O_3 and $LaMnO_3$. The U_{eff} values that result when these two compounds are concerned would differ by 0.22 eV for BEEF-vdW+U and 0.21 eV for PBE+U. The discrepancy is probably due to the fact that the magnetic structure of Mn_2O_3 has not yet been completely solved, especially when temperature is varied and, consequently, the collinear model proposed by Regulski et al. [50] was used in the present work, which is only a simple approximation based on powder neutron diffraction data measured at 10 K.

As for $LaCoO_3$, it may exhibit three different magnetic states, namely, low-spin (LS), immediate-spin (IS), and high-spin (HS) states [66]. The transition between the spin states of Co^{3+} at temperatures ranging from 90 to 600 K is still controversial [67]. Our calculations show that the IS state is the most stable magnetic state at room temperature, in good agreement with the experimental observations by Goodenough et al. [68-71], and the reason is probably due to the particularly strong d-p hybridization when Co^{3+} is in the IS state [72]. In addition, it is interesting to find that the U_{eff} value obtained increases from the LS to the IS, which can be explained by the requirement of additional energy to reduce the doubly occupied orbitals [73].

3.2.6 U_{eff} and ΔE_M values for 3d-block transition metals

Table 3. Calculated U_{eff} and ΔE_M values for 3*d*-block transition metals.

Transition metal	BEEF-vdW+U		PBE+U	
	U_{eff}	ΔE_M	U_{eff}	ΔE_M
Sc	0	0	0	0
Ti	0.6	0.07	1.3	0.32
V	2.5	1.40	3.0	1.53
Cr	2.5	1.38	3.0	1.53
Mn	3.5	1.27	4.7	1.72
Fe	2.9	1.46	4.8	1.98
Co	3.1	1.49	4.2	1.74
Ni	5.6	2.37	7.0	2.70
Cu	2.8	0.79	4.5	1.12

The calculated U_{eff} and ΔE_M values for the 3*d*-block transition metals are summarized in the Table 3. It can be seen from the table that the dependence of the U_{eff} on atomic number exhibits a non-monotonic behavior and follows nearly the same trend as that proposed by Wang et al. [4], regardless

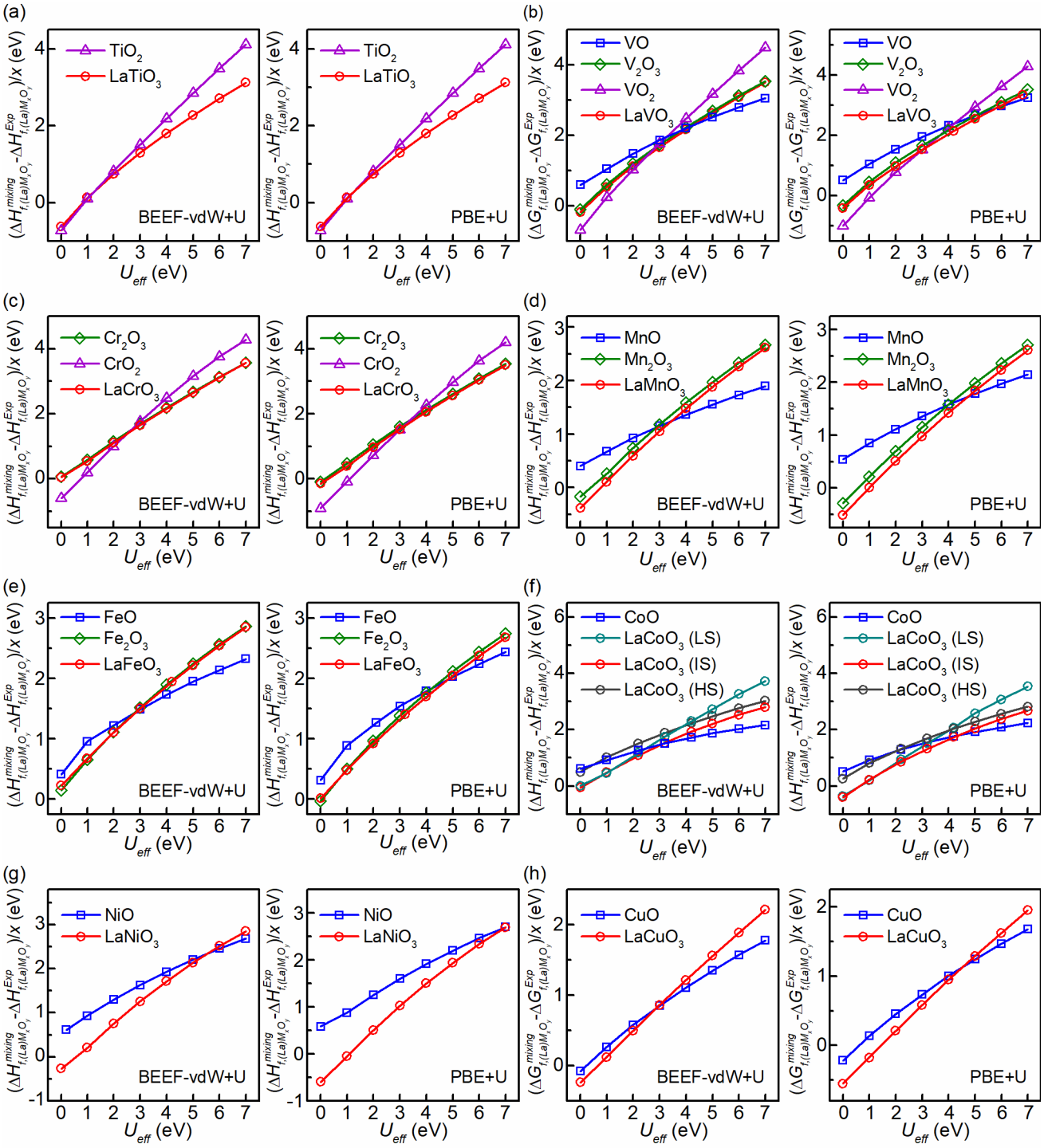

Figure 5. Differences between the calculated and experimental enthalpies or Gibbs free energies of formation of *Ti*-, *V*-, *Cr*-, *Mn*-, *Fe*-, *Co*-, *Ni*-, and *Cu*-based oxides as a function of U_{eff}

of the exchange-correlation functional used. The non-monotonic relationship has its origin in the non-monotonic behavior of the multiplet splitting as a function of atomic number. [74] Saitoh et al. calculated the U_{eff} values for $LaMO_3$ (M = *Ti*, *Cr*, *Mn*, *Fe*, and *Co*) by using a cluster model and suggested that the U_{eff} value for $LaFeO_3$ is largest because of the strongest Hund's rule-coupling stabilization in the d^5 configuration [74]. In addition, the U_{eff} values determined by using the BEEF-vdW method are generally smaller than those by PBE; that is, BEEF-vdW is capable of reducing the error in the calculated thermodynamic properties of transition-metal oxides, as compared to PBE. Interestingly, the training data sets used to optimize the BEEF-vdW method do not include any properties of strongly correlated systems. The improvement in the description of the electronic structures and energetics of transition-metal oxides lies in the fact that BEEF-vdW contains the vdW-DF2 nonlocal correlation functional as an essential component, which pairs

nonlocal correlation with LDA correlation and therefore includes semilocal correlation. [16]

It should be noted that the GGA+U method, although not entirely accurate in all details, provides an adequate and useful first description of the electronic structure of transition-metal oxides. By using the same U_{eff} values as determined in this work, Zheng et al. [75] and Li et al. [76] calculated the oxygen vacancy formation energies of $LaMO_3$ (M = *Sc* - *Cu*), which were found to agree well with available thermogravimetric data [77-79], even better than was obtained from the HSE06 hybrid functional [80]. On the other hand, within the GGA+U framework, all 3*d* electrons are driven to be more localized by adding a penalty function, where the strong hybridization between the e_g orbital and the *O* 2*p* states makes the e_g band less sensitive to the strength of the on-site Coulomb interaction than the t_{2g} orbital [58]. Hence, it is expected that excessive electron localization may persist in the e_g orbital. To ensure that the U_{eff} values determined by fitting the thermodynamic quantities can correctly reproduce other properties, the GGA+U method was used to calculate the structural, electronic, and magnetic properties of $LaMO_3$, which are then compared with available experimental data.

3.3 Properties of Perovskites

3.3.1 Lattice distortion

Unlike the ideal cubic perovskites, *La*-based perovskites $LaMO_3$ may adopt either an orthorhombic (*Sc* - *Fe*) or a rhombohedral (*Co* - *Cu*) structure at low temperatures, which results from the cooperative tiltings of MO_6 octahedra and the internal distortion due to the Jahn-Teller effect. It was reported that the octahedral rotation (GFO distortion) has a major effect on the ferromagnetic stability [81], band gap [82], and Mott transition [62] of materials. At room temperature, the MO_6 octahedra tilt in response to the size mismatch between the *La* and *M* cation, giving rise to low-symmetry lattice structures [83-86], with the *M-O-M* bond angle (θ_{M-O-M}) decreasing from 180 to 145 - 170 °. Therefore, the *M-O-M* bond angle can be used to some extent as a measure of the GFO distortion. Figure 6a depicts the variation of the average *M-O-M* bond angle in $LaMO_3$ as the atomic number of the constituent transition metals is changed, and the corresponding experimental data as well as the Goldschmidt tolerance factor are also presented for comparison. It can be seen that, although our calculated average *M-O-M* bond angles differ somewhat from the experimental data, they apparently follow the same trend. Interestingly, the Goldschmidt tolerance factor varies in much the way as well. The reason behind the resemblance is that both the *M-O-M* bond angle and the Goldschmidt tolerance factor of $LaMO_3$ depend solely on the effective ionic radius of the *M* cation, which can also be reflected in the cell volume. In figure 6b, the latter two structural parameters are presented and compared with the calculated cell volumes. Clearly, the GGA+U method tends to overestimate the cell volume, but the volume ordering is correctly predicted by the theoretical results. In particular, the cell volumes of $LaMnO_3$ and $LaFeO_3$ are abnormally larger

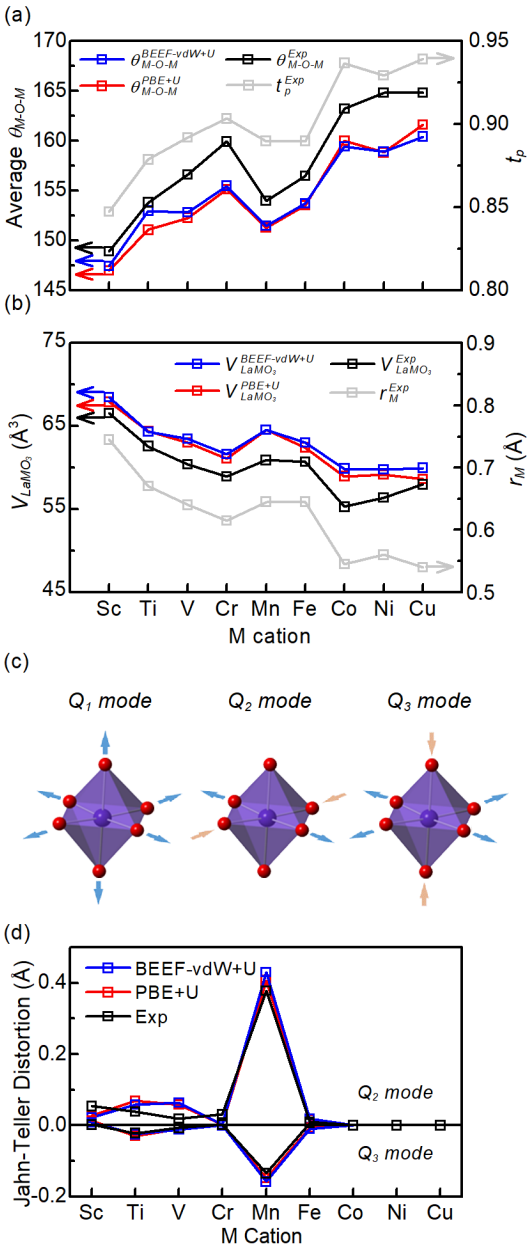

Figure 6. Calculated and experimental (a) average *M-O-M* bond angle, Goldschmidt tolerance factor, (b) cell volume of $LaMO_3$, and effective ionic radius of *M* at a function of the atomic number of the constituent transition metals in $LaMO_3$; (c). illustration of Q_1, Q_2, and Q_3 modes of the Jahn-Teller distortions in a MO_6 octahedron; (d). calculated and experimental Jahn-Teller distortion in $LaMO_3$.

than that of $LaCrO_3$, which can be explained by the balanced competition between the effects of the effective nuclear charge and the Coulomb repulsion in the 3*d* orbitals of these two materials [87].

As for the Jahn-Teller distortion, it has been found to have a pronounced effect on the metallicity and orbital ordering of perovskites by removing the degeneracy of *d* electrons and causing splitting of the *d* band [88]. The three basic modes of the Jahn-Teller distortion, namely, the breathing mode Q_1, the basal-plane distortion mode Q_2, and the octahedral stretching

mode Q_3, are illustrated in figure 6c. Since the Q_1 mode simply changes the volume of the MO_6 octahedron while retaining the symmetry of the materials, the Q_2 and Q_3 modes are often used to measure the degree of the Jahn-Teller distortion, which can be expressed in terms of the *M-O* bond lengths [87]

$$Q_2 = \sqrt{2} \cdot (l - s) \quad (15)$$

$$Q_3 = \frac{\sqrt{6} \cdot (2m - l - s)}{3} \quad (16)$$

where *s* and *l* are the short and long *M-O* bond lengths, respectively, pointing along the [100] and [010] axes, and *m* is the *M-O* bond length along the [001] axis, which is always less than or equal to *l*. The calculated and experimental Jahn-Teller distortions are shown in figure 6d. It is important to note that $LaCoO_3$, $LaNiO_3$, and $LaCuO_3$ adopt the highly symmetric rhombohedral structure with the six *M-O* bond lengths taking the same value and do not undergo the Jahn-Teller distortion. From Figure 6d, one can see that although DFT and DFT+U are known to deal with the structures and energies at absolute zero, our calculations based on the crystal and magnetic structures at room temperature may give results that are in remarkably good agreement with the experimental data.

3.3.2 Band structure

According to the difference between the on-site Coulomb repulsion energy which separates lower and upper Hubbard bands and the charge-transfer energy required to transfer an electron from the anion valence band to the *d* orbitals at the transition-metal site, *La*-based perovskites can be classified into three categories: $LaMO_3$ (*M* = *Sc*, *Cr*, *Fe*, and LS *Co*) are charge-transfer (CT) semiconductors, whose band gap is a *p-d* type gap between the anion 2*p* filled band and the *M* 3*d* upper Hubbard band; $LaMO_3$ (*M* = *Ti*, *Mn*, and *V*) are Mott-Hubbard insulators, whose band gap is a *d-d* type gap where the anion 2*p* band does not play a major role [40]; $LaNiO_3$ and $LaCuO_3$ are metallic conductors, with the filled lower Hubbard band overlapping the empty upper Hubbard band. The experimentally observed electrical conductivity and measured band gap of $LaMO_3$ are summarized in Table 4. The general decrease in the charge-transfer gap of the CT semiconductor from $LaScO_3$ to $LaCoO_3$ arises from the increased electronegativity of the metal cation [89].

To explore whether the U_{eff} values obtained can give a reasonably accurate description of the electrical conductivity of the perovskite materials, the band structure and density of states (DOS) of $LaMO_3$ are calculated by using the BEEF-vdW+U method, as shown in Figs 7 and 8, respectively. The calculated band gaps are listed in Table 4 and the corresponding data calculated by using the PBE method are given in the Supplementary Data. From figure 7, it can be seen that $LaScO_3$ has a direct band gap, in agreement with the previous calculations [90] where the calculated band gap by BEEF-vdW is over 2 eV smaller than the experimental value. The significant error in the calculated band gap is derived from the underestimation of the *Sc* 3*d* unoccupied band energy and can only be corrected when a large and unreasonable U_{eff} value is used, because the U_{eff} has a negligible effect on the band gap determined by the unoccupied *d* or *f* state [91]. As for $LaTiO_3$ which has a *d-d* type gap (see figure 8 for details), PBE+U overestimates the band gap by ~0.2 eV. By contrast, although the U_{eff} value seems too small to split the *Ti* 3*d* bands in the BEEF-vdW+U method, which results in the *Ti* unoccupied 3*d* band crossing the Fermi level, BEEF-vdW+U gives a more accurate energy gap (0.05 eV) between *Ti* 3*d* bands.

Table 4. Electrical conductivity and band gap of $LaMO_3$ (*M* = *Sc* – *Cu*).

Perovskite	Electrical conductivity	Band gap (eV)			
		Experimental	Calculated		
			BEEF-vdW+U	PBE+U	HSE
$LaScO_3$	CT semiconductor	5.7 [92], 6.0 [59]	3.83	3.92	5.73 [87]
$LaTiO_3$	MH insulator	0.1 [59], 0.2 [63]	0	0.35	1.27 [93] ,0.81 [87]
$LaVO_3$	MH insulator	1.1 [94]	1.34	1.47	1.46 [87]
$LaCrO_3$	CT semiconductor	3.4 [59]	2.69	2.80	3.00 [87], 3.06 [95]
$LaMnO_3$	MH insulator	1.1 [59], 1.7 [96], 1.9 [97], 2.0 [98]	1.04	1.18	1.63 [87], 1.52 [99],1.48 [100]
$LaFeO_3$	CT semiconductor	2.1 [59], 2.4 [101]	2.02	2.58	2.46 [87], 3.25 [95]
$LaCoO_3$	CT semiconductor (LS)	0.3 [59] (LS)	0 (IS)	0 (IS)	0.16 [87] (LS)
$LaNiO_3$	metal	0 [59]	0	0	-
$LaCuO_3$	metal	0 [59]	0	0	-

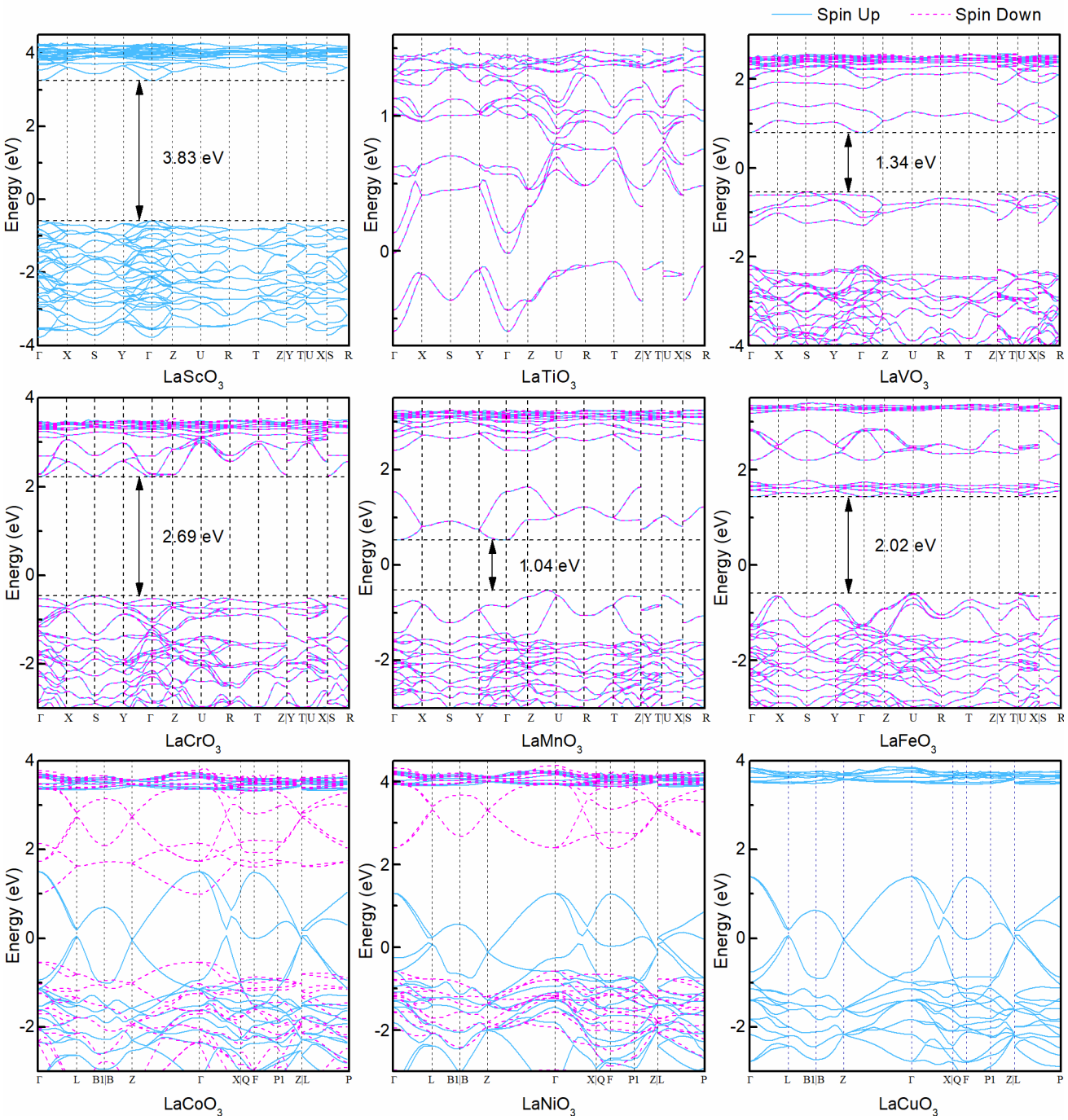

Figure 7. Calculated band structures of $LaMO_3$ ($M = Sc - Cu$) by BEEF-vdW+U.

The band gap of $LaVO_3$ is estimated by applying the U_{eff} values determined from the thermodynamic properties of VO_2 and $LaVO_3$ (2.5 eV for BEEF-vdW and 3.0 eV for PBE) as well as those of VO and $LaVO_3$ (4.2 eV for BEEF-vdW and 5.8 eV for PBE). The calculated results indicate that the lower U_{eff} values may give the band gap energies (1.34 eV for BEEF-vdW and 1.47 eV for PBE) that are comparable to the experimental value (1.1 eV). Like $LaTiO_3$, $LaVO_3$ has a *d-d* type band gap, which is also overestimated by over 0.37 eV by PBE+U. By comparison, BEEF-vdW+U that has a smaller U_{eff} value can reduce the error by 0.13 eV. From figure 7 and 8, it is clear that $LaCrO_3$ has a calculated *d-d* type band gap of 2.69 and 2.80 eV by BEEF-vdW+U and PBE+U, respectively. However, it was experimentally reported that $LaCrO_3$ is a CT insulator with a *p-d* gap of 3.4 eV [59]. The discrepancy is probably due to the fact that the U_{eff} value is not large enough for the *O* 2*p* band to lie above the *Cr* 3*d* sub-band and hence at the top of the valence band [102]

As can be seen from the density of spin-up and spin-down states of $LaCoO_3$ and $LaNiO_3$ in figure 8, they both behave as

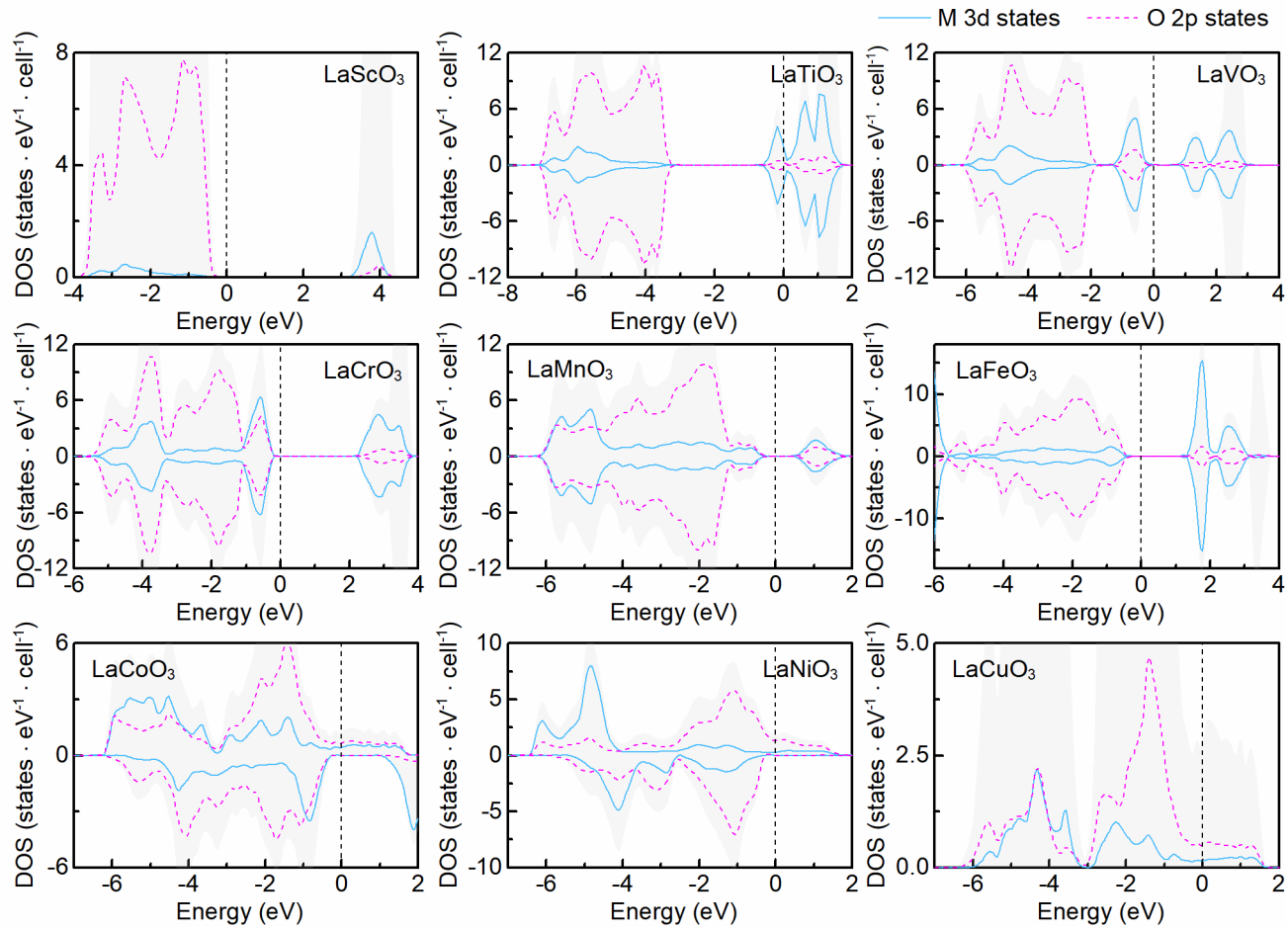

Figure 8. Calculated DOSs of $LaMO_3$ ($M = Sc - Cu$) by BEEF-vdW+U.

half-metals, in accord with previous calculations [72, 103, 104]. In experiment, however, $LaCoO_3$ and $LaNiO_3$ are predicted as a CT semiconductor and a metallic conductor, respectively, which can be explained by the LS *Co* cations in the experimentally used $LaCoO_3$ sample [67] and the excessive exchange splitting of the *Ni d* states by GGA [87]. For $LaMnO_3$, $LaFeO_3$, and $LaCuO_3$, both BEEF-vdW+U and PBE+U can give reasonably accurate *d-d* and *p-d* type band gaps or correctly reproduce the *Cu* 3*d* and *O* 2*p* bands crossing the Fermi level. Comparison between our calculated band gaps with previously reported results by HSE indicates the BEEF-vdW+U method shows a reasonable accuracy (see table 4). Although an improvement in the calculated band gap of $LaScO_3$ can only be achieved by using the hybrid functional (5.73 eV) with a mixing parameter [87], HSE gives larger errors in the calculated band gaps of $LaTiO_3$, $LaVO_3$, and $LaFeO_3$ than BEEF-vdW+U.

To further examine whether the fitted U_{eff} can be extrapolated to other oxides, the band gaps of most of binary 3*d*-block transition-metal oxides were also calculated compared with available experimental data, as summarized in Table S1. Since the U_{eff} values determined in the present work are based on the thermodynamic quantities of both binary and ternary oxides, it is reasonable to expect that the U_{eff} values may give a reasonably accurate description of the physical properties of the binary oxides. Indeed, one can see from the table that the calculated results agree reasonably with the experimental data, except for Sc_2O_3, TiO_2, and *VO*. The reason the band gaps of Sc_2O_3 and TiO_2 are much smaller than the experimental values is that introduction of a penalty function has a negligible effect on the energies of the occupied *O 2p* states and the unoccupied metal *3d* states. As for *VO*, because the U_{eff} value for *V* in $LaVO_3$ is determined by the thermodynamic and electronic properties of $LaVO_3$ and VO_2, it is not surprising to learn that the band gap of *VO* which has more localized *d* electrons is overestimated. To summarize, the transferability of U_{eff} across various binary oxides, especially to those containing the late transition metals, is satisfactory.

3.3.3 Magnetic moment

The variation in the magnetic moments of $LaMO_3$ can be readily understood in terms of the progressive filling of the t_{2g} and e_g bands. The magnetic configurations, the experimental and calculated magnetic moments of the perovskites are listed in Table 5, and the corresponding values of binary metal oxides are given in Table S1. It can be seen that the magnetic moment of $LaMO_3$ ($M = Sc$ - Fe) increases

Table 5. Magnetic configuration and magnetic moment of $LaMO_3$ ($M = Sc - Cu$).

Perovskite	Magnetic configuration of M^{3+}	Magnetic moment (μ_B)			
		Experimental	Calculated		
			BEEF-vdW+U	PBE+U	HSE
$LaScO_3$	d^0	0 [38]	0	0	0 [87]
$LaTiO_3$	$t_{2g}^{\uparrow}$	0.45 [105], 0.57 [106]	0.62	0.73	0.79 [87], 0.94 [93]
$LaVO_3$	$t_{2g}^{\uparrow\uparrow}$	1.3 [59]	1.81	1.82	1.82 [87]
$LaCrO_3$	$t_{2g}^{\uparrow\uparrow\uparrow}$	2.45 [107], 2.49 [108], 2.8 [109]	2.83	2.84	2.79 [87],
$LaMnO_3$	$t_{2g}^{\uparrow\uparrow\uparrow}e_g^{\uparrow}$	3.42 [110], 3.7 [111], 3.87 [112]	3.9	3.9	3.67 [87, 99], 3.8 [100]
$LaFeO_3$	$t_{2g}^{\uparrow\uparrow\uparrow}e_g^{\uparrow\uparrow}$	3.9 [113]	4.05	4.18	4 [87], 4.1 [114]
$LaCoO_3$	$t_{2g}^{\uparrow\downarrow\uparrow\downarrow\uparrow\downarrow}$ (LS)	0 [115] (LS)	2.11 (IS)	2.18 (IS)	0 [87] (LS), 1 [116] (IS)
$LaNiO_3$	$t_{2g}^{\uparrow\downarrow\uparrow\downarrow\uparrow\downarrow}e_g^{\uparrow}$	1 [117, 118]	1.41	1.49	-
$LaCuO_3$	$t_{2g}^{\uparrow\downarrow\uparrow\downarrow\uparrow\downarrow}e_g^{\uparrow\downarrow}$	0 [119]	0	0	-

as the transition-metal ion has more unpaired electrons, and the calculated values by BEEF-vdW+U and PBE+U agree well with the experiment data as well as those by HSE (see Tables 5 and S1). The only exception occurs for $LaCoO_3$. Although several DFT calculations [28, 115] have demonstrated that the IS $LaCoO_3$ is lower in energy than the LS $LaCoO_3$, the magnetic moment was measured under experimental conditions for which $LaCoO_3$ is in the nonmagnetic state [115]. It is important to note that the magnetic moments determined by BEEF-vdW+U compare more closely to the experimental data than those by the PBE+U method, which can be attributed to the smaller U_{eff} values used by the former, in the sense that the larger U_{eff} values may increase more dramatically the calculated magnetic moment by increasing the occupancy of spin-up ($t_{2g}^{\uparrow}$ and $e_g^{\uparrow}$) bands and by reducing the occupancy of spin-down electrons in the occupied states [102].

4. CONCLUSION

In this study, periodic DFT+U calculations have been carried out to study the thermodynamic, structural, electronic, and magnetic properties of *La*-based perovskites, with the use of the recently developed BEEF-vdW method and the most widely used PBE method. The "self-interaction error" in the occupied states of these strongly correlated systems is removed by introducing an effective interaction parameter U_{eff}, which is determined together with an energy adjustment ΔE_M by a mixing GGA and GGA+U method. In this method, the enthalpy or Gibbs free energy of formation of oxides containing a transition metal in different oxidation states is fitted to available experimental data, and the ΔE_M is found to have its origin in the fact that the GGA+U method gives rise to the offsets in the total energy that include not only the transition metal and does not vary with the identity of transition-metal oxides.

To ensure that the derived U_{eff} values can correctly reproduce other physical properties of $LaMO_3$, lattice distortion, band structure, and magnetic moment are calculated by using the derived U_{eff} values and compared with experimentally reported data. Calculated results indicate that the BEEF-vdW method provides a more accurate description of the bonding in the O_2 molecule than the PBE method and has generally smaller U_{eff} values for the 3*d*-block transition metals, thereby leading to band gaps and magnetic moments that are in better agreement with the experimentally measured values.

ACKNOWLEDGEMENTS

This work is supported by the Natural Science Foundation of China (21473053, 91645122, and U1663221), the National Key Research and Development Program of China

(2018YFB0604700), and the Fundamental Research Funds for the Central Universities (222201718003).

References

[1] Cohen A J, Mori-Sánchez P and Yang W 2012 Challenges for Density Functional Theory *Chem. Rev.* **112** 289-320
[2] Cohen A J, Mori-Sánchez P and Yang W 2008 Insights into Current Limitations of Density Functional Theory *Science* **321** 792-4
[3] Mori-Sánchez P, Cohen A J and Yang W 2008 Localization and Delocalization Errors in Density Functional Theory and Implications for Band-Gap Prediction *Phys. Rev. Lett.* **100** 146401
[4] Wang L, Maxisch T and Ceder G 2006 Oxidation energies of transition metal oxides within the GGA+U framework *Phys. Rev. B* **73** 195107
[5] Anisimov V I, Zaanen J and Andersen O K 1991 Band theory and Mott insulators: Hubbard U instead of Stoner I *Phys. Rev. B* **44** 943-54
[6] Anisimov V I, Aryasetiawan F and Lichtenstein A I 1997 First-principles calculations of the electronic structure and spectra of strongly correlated systems: the LDA + U method *J. Phys.: Condens. Matter* **9** 767
[7] Heyd J, Scuseria G E and Ernzerhof M 2003 Hybrid functionals based on a screened Coulomb potential *J. Chem. Phys.* **118** 8207-15
[8] Ren X, Rinke P, Joas C and Scheffler M 2012 Random-phase approximation and its applications in computational chemistry and materials science *J. Mater. Sci.* **47** 7447-71
[9] Dudarev S L, Botton G A, Savrasov S Y, Humphreys C J and Sutton A P 1998 Electron-energy-loss spectra and the structural stability of nickel oxide: An LSDA+U study *Phys. Rev. B* **57** 1505-9
[10] Cococcioni M and de Gironcoli S 2005 Linear response approach to the calculation of the effective interaction parameters in the LDA+U method *Phys. Rev. B* **71** 035105
[11] Loschen C, Carrasco J, Neyman K M and Illas F 2007 First-principles LDA+U and GGA+U study of cerium oxides: Dependence on the effective U parameter *Phys. Rev. B* **75** 035115
[12] Hu Z and Metiu H 2011 Choice of U for DFT+U Calculations for Titanium Oxides *J. Phys. Chem. C* **115** 5841-5
[13] Hashemifar T, Mokhtari A and Soleimanian V 2017 Electronic, Structural and Magnetic Properties of the Sr_2CoWO_6 Double Perovskite Using GGA (+U) *J. Supercond. Novel Magn.* **30** 497-503
[14] Rezaiguia M, Benstaali W, Abbad A, Bentata S and Bouhafs B 2017 GGA + U Study of Electronic and Magnetic Properties of $Pr(Fe/Cr)O_3$ Cubic Perovskites *J. Supercond. Novel Magn.* **30** 2581-90
[15] Aykol M and Wolverton C 2014 Local environment dependent GGA+U method for accurate thermochemistry of transition metal compounds *Phys. Rev. B* **90** 115105
[16] Wellendorff J, Lundgaard K T, Møgelhøj A, Petzold V, Landis D D, Nørskov J K, Bligaard T and Jacobsen K W 2012 Density functionals for surface science: Exchange-correlation model development with Bayesian error estimation *Phys. Rev. B* **85** 235149
[17] Perdew J P and Wang Y 1992 Accurate and simple analytic representation of the electron-gas correlation energy *Phys. Rev. B* **45** 13244-9
[18] Perdew J P, Burke K and Ernzerhof M 1996 Generalized Gradient Approximation Made Simple *Phys. Rev. Lett.* **77** 3865-8
[19] Lee K, Murray É D, Kong L, Lundqvist B I and Langreth D C 2010 Higher-accuracy van der Waals density functional *Phys. Rev. B* **82** 081101
[20] De Angelis F, Di Valentin C, Fantacci S, Vittadini A and Selloni A 2014 Theoretical Studies on Anatase and Less Common TiO_2 Phases: Bulk, Surfaces, and Nanomaterials *Chem. Rev.* **114** 9708-53
[21] Adler S B 2004 Factors Governing Oxygen Reduction in Solid Oxide Fuel Cell Cathodes *Chem. Rev.* **104** 4791-844
[22] Royer S, Duprez D, Can F, Courtois X, Batiot-Dupeyrat C, Laassiri S and Alamdari H 2014 Perovskites as Substitutes of Noble Metals for Heterogeneous Catalysis: Dream or Reality *Chem. Rev.* **114** 10292-368
[23] Gupta S, Mahapatra M K and Singh P 2015 Lanthanum chromite based perovskites for oxygen transport membrane *Mater. Sci. Eng.* **90** 1-36
[24] Fergus J W 2007 Perovskite oxides for semiconductor-based gas sensors *Sens. Actuators, B* **123** 1169-79
[25] Usman T, Murtaza G, Luo H J and Mahmood A 2017 GGA and GGA plus U Study of Rare Earth-Based Perovskites in Cubic Phase *J. Supercond. Novel Magn.* **30** 1389-96
[26] Piyanzina I I, Kopp T, Lysogorskiy Y V, Tayurskii D A and Eyert V 2017 Electronic properties of $LaAlO_3/SrTiO_3$ n-type interfaces: a GGA plus U study *Journal of Physics: Condensed Matter* **29**
[27] Dar S A, Srivastava V and Sakalle U K 2017 A combined DFT and post-DFT investigation on cubic $XMoO_3$ (X = Sr, Ba) perovskite oxides *Mater. Res. Express* **4** 12
[28] Wang X, Han Y, Song X, Liu W and Cui H 2017 Phonon spectrum and thermodynamic properties of $LaCoO_3$ based on first-principles theory *Comp. Mater. Sci.* **136** 191-7
[29] Zhang J, Ji C, Shangguan Y, Guo B, Wang J, Huang F, Lu X and Zhu J 2018 Strain-driven magnetic phase transitions from an antiferromagnetic to a ferromagnetic state in perovskite $RMnO_3$ films *Phys. Rev. B* **98** 195133
[30] Boateng I W, Tia R, Adei E, Dzade N Y, Catlow C R A and De Leeuw N H 2017 A DFT plus U investigation of hydrogen adsorption on the LaFeO3(010) surface *PCCP* **19** 7399-409
[31] Kresse G and Furthmüller J 1996 Efficiency of ab-initio total energy calculations for metals and semiconductors using a plane-wave basis set *Comp. Mater. Sci.* **6** 15-50
[32] Blöchl P E 1994 Projector augmented-wave method *Phys. Rev. B* **50** 17953-79
[33] Monkhorst H J and Pack J D 1976 Special points for Brillouin-zone integrations *Phys. Rev. B* **13** 5188-92
[34] Zhu Y-A, Chen D, Zhou X-G and Yuan W-K 2009 DFT studies of dry reforming of methane on Ni catalyst *Catal. Today* **148** 260-7
[35] Jain A, Hautier G, Ong S P, Moore C J, Fischer C C, Persson K A and Ceder G 2011 Formation enthalpies by mixing GGA and GGA+ U calculations *Phys. Rev. B* **84** 045115
[36] Xu Z, Joshi Y V, Raman S and Kitchin J R 2015 Accurate electronic and chemical properties of 3d transition metal oxides using a calculated linear response U and a DFT + U(V) method *J. Chem. Phys.* **142** 144701
[37] Haynes W M 2013 *CRC handbook of chemistry and physics*: CRC press)
[38] Muñoz A, Alonso J A, Casáis M T, Martínez-Lope M J, Martínez J L and Fernández-Díaz M T 2003

Crystallographic and magnetic transitions in $CeVO_3$: A neutron diffraction study *Phys. Rev. B* **68** 144429
[39] Cheng J and Navrotsky A 2003 Enthalpies of formation of $LaBO_3$ perovskites (B= Al, Ga, Sc, and In) *J. Mater. Res.* **18** 2501-8
[40] Fujimori A and Tokura Y 1994 *Spectroscopy of Mott Insulators and Correlated Metals* vol 119: Springer Science & Business Media)
[41] Cheng Z, Zha S and Liu M 2006 Stability of Materials as Candidates for Sulfur-Resistant Anodes of Solid Oxide Fuel Cells *J. Electrochem. Soc.* **153** A1302-A9
[42] Yokokawa H, Sakai N, Kawada T and Dokiy M 1990 Chemical Potential Diagrams for Rare Earth-Transition Metal-Oxygen Systems: I, Ln-V-O and Ln-Mn-O System *J. Am. Ceram. Soc.* **73** 649-58
[43] Cheng J, Navrotsky A, Zhou X-D and Anderson H U 2011 Enthalpies of Formation of $LaMO_3$ Perovskites (M = Cr, Fe, Co, and Ni) *J. Mater. Res.* **20** 191-200
[44] Sreedharan O M, Mallika C and Swaminathan K 1988 Estimation of oxygen pressures for the formation of superconducting phases based on La-Cu-O and Y-Cu-O systems *J. Mater. Sci.* **23** 2735-9
[45] Adler D 1968 Mechanisms for Metal-Nonmental Transitions in Transition-Metal Oxides and Sulfides *Rev. Mod. Phys.* **40** 714-36
[46] Balcar E and Lovesey S W 2002 Neutron diffraction by magnetic crystals: V_2O_3 *J. Phys.: Condens. Matter* **14** 10281-93
[47] Corliss L M, Hastings J M, Nathans R and Shirane G 1965 Magnetic structure of Cr_2O_3 *J. Appl. Phys.* **36** 1099-100
[48] Sivakumar V, Ross C A, Yabuuchi N, Shao-Horn Y, Persson K and Ceder G 2008 Electrochemical Control of the Magnetic Moment of CrO_2 *J. Electrochem. Soc.* **155** P83-P8
[49] Roth W L 1958 Magnetic structures of MnO, FeO, CoO, and NiO *Phys. Rev.* **110** 1333
[50] Regulski M, Przeniosło R, Sosnowska I, Hohlwein D and Schneider R 2004 Neutron diffraction study of the magnetic structure of α-Mn_2O_3 *J. Alloys Compd.* **362** 236-40
[51] Jauch W, Reehuis M, Bleif H J, Kubanek F and Pattison P 2001 Crystallographic symmetry and magnetic structure of CoO *Phys. Rev. B* **64** 052102
[52] Ain M, Menelle A, Wanklyn B and Bertaut E 1992 Magnetic structure of CuO by neutron diffraction with polarization analysis *J. Phys.: Condens. Matter* **4** 5327
[53] Gale W F and Totemeier T C 2003 *Smithells metals reference book*: Butterworth-Heinemann)
[54] Wilson J A 2007 A negative-U interpretation of the femtosecond laser pulse-induced crystallographic expansion of a cuprate HTSC material reported recently by Gedik et al *J. Phys.: Condens. Matter* **19** 466210
[55] Pena M A and Fierro J L G 2001 Chemical structures and performance of perovskite oxides *Chem. Rev.* **101** 1981-2018
[56] Sreedharan O M, Chandrasekharaiah M S and Karkhanavala M D 1977 Thermodynamic stabilities of cobalt oxides *High Temp. Sci.* **9** 109-18
[57] Pople J A, Head-Gordon M, Fox D J, Raghavachari K and Curtiss L A 1989 Gaussian-1 theory: A general procedure for prediction of molecular energies *J. Chem. Phys.* **90** 5622-9
[58] Solovyev I, Hamada N and Terakura K 1996 t_{2g} versus all 3d localization in $LaMO_3$ perovskites (M=Ti-Cu): First-principles study *Phys. Rev. B* **53** 7158-70
[59] Arima T, Tokura Y and Torrance J B 1993 Variation of optical gaps in perovskite-type 3d transition-metal oxides *Phys. Rev. B* **48** 17006-9
[60] Arrio M A, Rossano S, Ch B, Galoisy L and Calas G 2000 Calculation of multipole transitions at the Fe K pre-edge through p - d hybridization in the Ligand Field Multiplet model *Europhys. Lett.* **51** 454
[61] Khaliullin G and Maekawa S 2000 Orbital Liquid in Three-Dimensional Mott Insulator: $LaTiO_3$ *Phys. Rev. Lett.* **85** 3950-3
[62] Pavarini E, Biermann S, Poteryaev A, Lichtenstein A I, Georges A and Andersen O K 2004 Mott Transition and Suppression of Orbital Fluctuations in Orthorhombic $3d^1$ Perovskites *Phys. Rev. Lett.* **92** 176403
[63] Okimoto Y, Katsufuji T, Okada Y, Arima T and Tokura Y 1995 Optical spectra in $(La,Y)TiO_3$ Variation of Mott-Hubbard gap features with change of electron correlation and band filling *Phys. Rev. B* **51** 9581-8
[64] Biscaras J, Bergeal N, Kushwaha A, Wolf T, Rastogi A, Budhani R C and Lesueur J 2010 Two-dimensional superconductivity at a Mott insulator/band insulator interface $LaTiO_3/SrTiO_3$ *Nat. Commun.* **1** 89
[65] Lutfalla S, Shapovalov V and Bell A T 2011 Calibration of the DFT/GGA+ U method for determination of reduction energies for transition and rare earth metal oxides of Ti, V, Mo, and Ce *J. Chem. Theory Comput.* **7** 2218-23
[66] Señarís-Rodríguez M A and Goodenough J B 1995 Magnetic and Transport Properties of the System $La_{1-x}Sr_xCoO_{3-\delta}$ ($0 \le x \le 0.50$) *J. Solid State Chem.* **118** 323-36
[67] Laref A, Laref S and Bin-Omran S 2012 Electronic structure, X-ray absorption, and optical spectroscopy of $LaCoO_3$ in the ground-state and excited-states *J. Comput. Chem.* **33** 673-84
[68] Goodenough J B 1958 An interpretation of the magnetic properties of the perovskite-type mixed crystals $La_{1-x}Sr_xCoO_{3-\lambda}$ *J. Phys. Chem. Solids* **6** 287-97
[69] Zhou J S, Yan J Q and Goodenough J B 2005 Bulk modulus anomaly in $RCoO_3$ (R=La, Pr, and Nd) *Phys. Rev. B* **71** 220103
[70] Yan J Q, Zhou J S and Goodenough J B 2004 Bond-length fluctuations and the spin-state transition in $LCoO_3$ (L=La, Pr, and Nd) *Phys. Rev. B* **69** 134409
[71] Radaelli P G and Cheong S W 2002 Structural phenomena associated with the spin-state transition in $LaCoO_3$ *Phys. Rev. B* **66** 094408
[72] Korotin M A, Ezhov S Y, Solovyev I V, Anisimov V I, Khomskii D I and Sawatzky G A 1996 Intermediate-spin state and properties of $LaCoO_3$ *Phys. Rev. B* **54** 5309
[73] Fulde P 2012 *Electron correlations in molecules and solids* vol 100: Springer Science & Business Media)
[74] Saitoh T, Bocquet A E, Mizokawa T and Fujimori A 1995 Systematic variation of the electronic structure of 3d transition-metal compounds *Phys. Rev. B* **52** 7934-8
[75] Zheng Y-S, Zhang M, Li Q, Zhu Y, Sui Z J, Chen D and Zhou X 2018 Electronic Origin of Oxygen Transport Behavior in La-Based Perovskites: A Density Functional Theory Study *J. Phys. Chem. C* accepted
[76] Li Q, Deng Y-X, Zhu Y-A, Li Y, Sui Z-J, Chen D and Yuan W-K 2018 Structural stability of Lanthanum-based oxygen-deficient perovskites in redox catalysis: A density functional theory study *Catal. Today* accepted
[77] Nowotny J and Rekas M 1998 Defect Chemistry of $(La,Sr)MnO_3$ *J. Am. Ceram. Soc.* **81** 67-80
[78] Mizusaki J, Yoshihiro M, Yamauchi S and Fueki K 1985 Nonstoichiometry and defect structure of the

perovskite-type oxides $La_{1-x}Sr_xFeO_{3-\delta}$ *J. Solid State Chem.* **58** 257-66
[79] Mizusaki J, Mima Y, Yamauchi S, Fueki K and Tagawa H 1989 Nonstoichiometry of the perovskite-type oxides $La_{1-x}Sr_xCoO_{3-\delta}$ *J. Solid State Chem.* **80** 102-11
[80] Pavone M, Ritzmann A M and Carter E A 2011 Quantum-mechanics-based design principles for solid oxide fuel cell cathode materials *Energy Environ. Sci.* **4** 4933-7
[81] Middey S, Mahadevan P and Sarma D D 2011 Dependence of magnetism on $GdFeO_3$ distortion in the t_{2g} system $ARuO_3$ (A = Sr, Ca) *Phys. Rev. B* **83** 014416
[82] Mizokawa T and Fujimori A 1996 Electronic structure and orbital ordering in perovskite-type 3d transition-metal oxides studied by Hartree-Fock band-structure calculations *Phys. Rev. B* **54** 5368-80
[83] Smirnov A M, Estemirova S K and Karpasyuk V K 2011 Structural and magnetic characteristics of manganites in $La_{1-c+x}Sr_{c-x}Mn_{1-x}Ni_xO_3$ system. In: *J. Phys. Conf. Ser.*: IOP Publishing) p 012071
[84] Gupta S, Tomar M and Gupta V 2014 Study on Mn-induced Jahn–Teller distortion in $BiFeO_3$ thin films *J. Mater. Sci.* **49** 5997-6006
[85] Kayser P, Martínez-Lope M J, Alonso J A, Retuerto M, Croft M, Ignatov A and Fernández-Díaz M T 2013 Crystal Structure, Phase Transitions, and Magnetic Properties of Iridium Perovskites Sr_2MIrO_6 (M = Ni, Zn) *Inorg. Chem.* **52** 11013-22
[86] Rui Z, Ding J, Li Y and Lin Y S 2010 $SrCo_{0.8}Fe_{0.2}O_{3-\delta}$ sorbent for high-temperature production of oxygen-enriched carbon dioxide stream *Fuel* **89** 1429-34
[87] He J and Franchini C 2012 Screened hybrid functional applied to $3d^0 \rightarrow 3d^8$ transition-metal perovskites $LaMO_3$ (M=Sc–Cu) : Influence of the exchange mixing parameter on the structural, electronic, and magnetic properties *Phys. Rev. B* **86** 235117
[88] Maris G, Ren Y, Volotchaev V, Zobel C, Lorenz T and Palstra T T M 2003 Evidence for orbital ordering in $LaCoO_3$ *Phys. Rev. B* **67** 224423
[89] Bocquet A E, Mizokawa T, Morikawa K, Fujimori A, Barman S R, Maiti K, Sarma D D, Tokura Y and Onoda M 1996 Electronic structure of early 3d-transition-metal oxides by analysis of the 2p core-level photoemission spectra *Phys. Rev. B* **53** 1161
[90] Pari G, Mathi Jaya S, Subramoniam G and Asokamani R 1995 Density-functional description of the electronic structure of $LaMO_3$ (M = Sc, Ti, V, Cr, Mn, Fe, Co, Ni) *Phys. Rev. B* **51** 16575-81
[91] Jiang H, Gomez-Abal R I, Rinke P and Scheffler M 2009 Localized and Itinerant States in Lanthanide Oxides United by GW @ LDA+U *Phys. Rev. Lett.* **102** 126403
[92] Afanas'ev V V, Stesmans A, Zhao C, Caymax M, Heeg T, Schubert J, Jia Y, Schlom D G and Lucovsky G 2004 Band alignment between (100)Si and complex rare earth/transition metal oxides *Appl. Phys. Lett.* **85** 5917-9
[93] El-Mellouhi F, Brothers E N, Lucero M J, Bulik I W and Scuseria G E 2013 Structural phase transitions of the metal oxide perovskites $SrTiO_3$, $LaAlO_3$, and $LaTiO_3$ studied with a screened hybrid functional *Phys. Rev. B* **87** 035107
[94] Zubkov V G, Bazuev G V, Perelyae V A and Shveikin G P 1973 Magnetic structure of $LaVO_3$ *Sov. Phys. Solid Stateddd* **15** 1078
[95] Hong J, Stroppa A, Íñiguez J, Picozzi S and Vanderbilt D 2012 Spin-phonon coupling effects in transition-metal perovskites: A DFT + U and hybrid-functional study *Phys. Rev. B* **85** 054417
[96] Saitoh T, Bocquet A E, Mizokawa T, Namatame H, Fujimori A, Abbate M, Takeda Y and Takano M 1995 Electronic structure of $La_{1-x}Sr_xMnO_3$ studied by photoemission and x-ray-absorption spectroscopy *Phys. Rev. B* **51** 13942-51
[97] Jung J H, Kim K H, Eom D J, Noh T W, Choi E J, Yu J, Kwon Y S and Chung Y 1997 Determination of electronic band structures of $CaMnO_3$ and $LaMnO_3$ using optical-conductivity analyses *Phys. Rev. B* **55** 15489-93
[98] Krüger R, Schulz B, Naler S, Rauer R, Budelmann D, Bäckström J, Kim K H, Cheong S W, Perebeinos V and Rübhausen M 2004 Orbital ordering in $LaMnO_3$ Investigated by Resonance Raman Spectroscopy *Phys. Rev. Lett.* **92** 097203
[99] Rivero P, Meunier V and Shelton W 2016 Electronic, structural, and magnetic properties of $LaMnO_3$ phase transition at high temperature *Phys. Rev. B* **93** 024111
[100] Gavin A L and Watson G W 2017 Modelling the electronic structure of orthorhombic LaMnO3 *Solid State Ionics* **299** 13-7
[101] Bellakki M B, Kelly B J and Manivannan V 2010 Synthesis, characterization, and property studies of (La, Ag) FeO_3 ($0.0 \leq x \leq 0.3$) perovskites *J. Alloys Compd.* **489** 64-71
[102] Yang Z, Huang Z, Ye L and Xie X 1999 Influence of parameters U and J in the LSDA+U method on electronic structure of the perovskites $LaMO_3$ (M=Cr, Mn, Fe, Co, Ni) *Phys. Rev. B* **60** 15674-82
[103] Knížek K, Jirák Z, Hejtmánek J and Novák P 2006 Character of the excited state of the Co^{3+} ion in $LaCoO_3$ *J. Phys.: Condens. Matter* **18** 3285
[104] Zhuang M, Zhang W and Ming N 1998 Competition of various spin states of $LaCoO_3$ *Phys. Rev. B* **57** 10705-9
[105] Goral J P and Greedan J E 1983 The magnetic structures of $LaTiO_3$ and $CeTiO_3$ *J. Magn. Magn. Mater.* **37** 315-21
[106] Cwik M, Lorenz T, Baier J, Müller R, André G, Bourée F, Lichtenberg F, Freimuth A, Schmitz R, Müller-Hartmann E and Braden M 2003 Crystal and magnetic structure of $LaTiO_3$: Evidence for nondegenerate t_{2g} orbitals *Phys. Rev. B* **68** 060401
[107] Koehler W C and Wollan E O 1957 Neutron-diffraction study of the magnetic properties of perovskite-like compounds $LaBO_3$ *J. Phys. Chem. Solids* **2** 100-6
[108] Sakai N, Fjellvâg H and Hauback B C 1996 Structural, Magnetic, and Thermal Properties of $La_{1-t}Ca_tCrO_{3-\delta}$ *J. Solid State Chem.* **121** 202-13
[109] Bertaut E F, Mareschal J, de Vries G, Aleonard R, Pauthenet R, Rebouillat J P and Zarubicka V 1966 Etude des propriétés magnétostatiques et des structures magnétiques des chromites des terres rares et d'yttrium *IEEE Trans. Magn.* **2** 453-8
[110] Hauback B C, Fjellvåg H and Sakai N 1996 Effect of Nonstoichiometry on Properties of $La_{1-t}MnO_{3+\delta}$: III. Magnetic Order Studied by Powder Neutron Diffraction *J. Solid State Chem.* **124** 43-51
[111] Elemans J B A A, Van Laar B, Van Der Veen K R and Loopstra B O 1971 The crystallographic and magnetic structures of $La_{1-x}Ba_xMn_{1-x}Me_xO_3$ (Me = Mn or Ti) *J. Solid State Chem.* **3** 238-42
[112] Moussa F, Hennion M, Rodriguez-Carvajal J, Moudden H, Pinsard L and Revcolevschi A 1996 Spin waves in the antiferromagnet perovskite $LaMnO_3$: A neutron-scattering study *Phys. Rev. B* **54** 15149-55
[113] Zhou X-D, Pederson L R, Cai Q, Yang J, Scarfino B J, Kim M, Yelon W B, James W J, Anderson H U and Wang C 2006 Structural and magnetic properties of $LaMn_{1-x}Fe_xO_3$ *J. Appl. Phys.* **99** 08M918

[114] Zhu Z, Peelaers H and Van de Walle C G 2017 Electronic and protonic conduction in $LaFeO_3$ *Journal of Materials Chemistry A: Materials for Energy and Sustainability* **5** 15367-79
[115] Stølen S, Grønvold F, Brinks H, Atake T and Mori H 1997 Energetics of the spin transition in $LaCoO_3$ *Phys. Rev. B* **55** 14103-6
[116] Zhang X-b, Gang F and Wan H-l 2014 Density Functional Theory Study on Spin States of $LaCoO_3$ at Room Temperature *Chinese Journal of Chemical Physics* **27** 274-8
[117] Goodenough J B and Raccah P M 1965 Complex vs Band Formation in Perovskite Oxides *J. Appl. Phys.* **36** 1031-2
[118] Huang K, Lee H Y and Goodenough J B 1998 Sr- and Ni-Doped $LaCoO_3$ and $LaFeO_3$ Perovskites: New Cathode Materials for Solid-Oxide Fuel Cells *J. Electrochem. Soc.* **145** 3220-7
[119] Bringley J F, Scott B A, La Placa S J, McGuire T R, Mehran F, McElfresh M W and Cox D E 1993 Structure and properties of the $LaCuO_{3-\delta}$ perovskites *Phys. Rev. B* **47** 15269-75

